Accepted Manuscript

Single crystal growth of CeTAl$_3$ (T = Cu, Ag, Au, Pd and Pt)

C. Franz, A. Senyshyn, A. Regnat, C. Duvinage, R. Schönmann, A. Bauer, Y. Prots, L. Akselrud, V. Hlukhyy, V. Baran, C. Pfleiderer

PII: S0925-8388(16)32104-1

DOI: 10.1016/j.jallcom.2016.07.071

Reference: JALCOM 38239

To appear in: *Journal of Alloys and Compounds*

Received Date: 8 April 2016

Revised Date: 4 July 2016

Accepted Date: 5 July 2016

Please cite this article as: C. Franz, A. Senyshyn, A. Regnat, C. Duvinage, R. Schönmann, A. Bauer, Y. Prots, L. Akselrud, V. Hlukhyy, V. Baran, C. Pfleiderer, Single crystal growth of CeTAl$_3$ (T = Cu, Ag, Au, Pd and Pt), *Journal of Alloys and Compounds* (2016), doi: 10.1016/j.jallcom.2016.07.071.

Single crystal growth of $CeTAl_3$ (T = Cu, Ag, Au, Pd and Pt)

C. Franz[a,b,*], A. Senyshyn[b], A. Regnat[a], C. Duvinage[a], R. Schönmann[a], A. Bauer[a], Y. Prots[c], L. Akselrud[c], V. Hlukhyy[d], V. Baran[d], C. Pfleiderer[a]

[a] *Physik Department, Technische Universität München, D-85747 Garching, Germany*
[b] *Heinz Maier-Leibnitz Zentrum (MLZ), Technische Universität München, D-85748 Garching, Germany*
[c] *Max-Planck Institut für die chemische Physik fester Stoffe (MPI CPFS), D-01187 Dresden, Germany*
[d] *Fakultät für Chemie, Technische Universität München, D-85747 Garching, Germany*

Abstract

We report single crystal growth of the series of $CeTAl_3$ compounds with T = Cu, Ag, Au, Pd and Pt by means of optical float zoning, where high crystal quality was confirmed in a thorough characterization process. With the exception of $CeAgAl_3$, all compounds crystallize in the non-centrosymmetric tetragonal $BaNiSn_3$ structure (space group: *I4mm*, No. 107), whereas $CeAgAl_3$ adopts the related orthorhombic $PbSbO_2Cl$ structure (Cmcm, No. 63). An attempt to grow $CeNiAl_3$ resulted in the composition $CeNi_2Al_5$. Low temperature resistivity measurements down to ∼0.1 K did not reveal evidence suggestive of magnetic order in $CePtAl_3$ and $CePdAl_3$. In contrast, $CeAuAl_3$, $CeCuAl_3$ and $CeAgAl_3$ display signatures of magnetic transitions at 1.3 K, 2.1 K and 3.2 K, respectively. This is consistent with previous reports of antiferromagnetic order in $CeAuAl_3$ and $CeCuAl_3$ as well as ferromagnetism in $CeAgAl_3$, respectively.

Keywords: float zone technique, single crystal growth, rare earth compounds, magnetic materials, crystal structure determination, electrical resistivity

1. Introduction

Cerium-based intermetallic compounds represent an ideal testing ground for the study of novel electronic ground states and unusual low-lying excitations, where valence fluctuations, heavy-fermion behaviour, unconventional superconductivity and exotic forms of spin and charge order are ubiquitous. Despite many decades of intense research, the understanding of the nature of strong electronic correlations in Ce-based systems is still rather qualitative. A scenario that is widely alluded to when addressing correlations in f-electron systems considers the competition of Ruderman-Kittel-Kasuya-Yosida (RKKY) interactions, supporting magnetic order, with the single-impurity Kondo effect quenching magnetic moments. While there have been various attempts to advance the understanding, simultaneous treatment of multiple, nearly equivalent energy scales such as exchange and dipolar interaction, spin-orbit coupling, crystal electric fields and strong magneto-elastic coupling has not been attempted.

Given this general context, the class of $CeTX_3$, where T is a transition metal element and X a simple metal, offer important new insights. For instance, selected members of this series have been discovered, which exhibit a coexistence of magnetic order and superconductivity under pressure. Another line of research pursues the strong coupling of phonons with relatively low lying crystal electric fields (CEF) levels. An important example has been reported in $CeCuAl_3$ [1], which was interpreted in terms of a quasi-bound vibron state first observed in $CeAl_2$ [2, 3]. However, recent studies in $CePd_2Al_2$, as well as preliminary work in other members of the $CeTX_3$ series suggest, that strong interactions of the crystal fields with the spectrum of phonons somewhat akin the claim of vibrons in $CeCuAl_3$, is more generic than assumed so far.

In this paper we report single crystal growth of

*Corresponding author. +49 89 289 14760
Email address: christian.franz@frm2.tum.de (C. Franz)

the series CeTAl$_3$ with T = Cu, Ag, Au, Pd and Pt. For our study we have used optical float zoning, to the best of our knowledge, for the first time in the class of CeTX_3 systems. This technique has been successfully used in different Ce-based systems, including $CeSi_{2-\sigma}$ [4], $CeCu_2Si_2$ [5] and $CeNi_2Ge_2$ [6]. Following a thorough characterisation, we determined the crystal structure of the systems studied. The high sample quality achieved in our study is corroborated in measurements of the electrical resistivity, which were performed at temperatures down to 0.1 K.

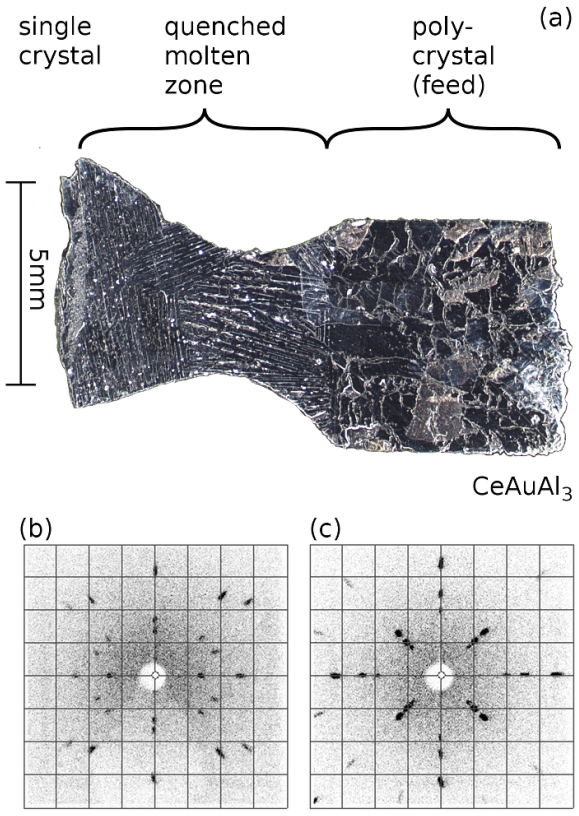

Figure 1: (a) Cut through the quenched final zone of the $CeAuAl_3$ crystal along the rotational symmetry axis. Polycrystalline part of the feed rod, quenched molten zone and beginning of the single crystal are visible. The quenched molten zone features a pronounced stripe pattern. Laue X-ray images along crystallographic a- and c-axes are shown in panels (b) and (c), respectively.

All crystal structures reported in the literature for the series of CeTAl$_3$ compounds are derived from the $BaAl_4$ structure, depicted in Fig. 2 (a). The $BaAl_4$ structure is tetragonally body-centred with eight Ce-atoms at the corners and one in the center. The aluminum atoms are arranged in six planes parallel to ab in the unit cell. The following three important types of structures may be derived from the $BaAl_4$ structure in which the Al and T atoms are ordered.

(i) The $ThCr_2Si_2$ (*I4/mmm*) structure, shown in Fig. 2 (b), has so far been most frequently reported for intermetallic compounds. The sequence of layers along the c-direction is given as A - [X-T-X] - A with A a rare-earth metal, T the transition metal element and X either Si, Ge or Al. Typical examples include CeT_2X_2 compounds ($CeCu_2Si_2$ [7], $CeCu_2Ge_2$ [8], $CePd_2Si_2$, $CeRh_2Si_2$ [9]) as well as URu_2Si_2 [10] and $BaFe_2As_2$ [11].

(ii) The $CaBe_2Ge_2$ (*P4/nmm*) variant of the $BaAl_4$ structure, shown in Fig. 2 (c), is also characterised by full inversion symmetry and a layered appearance along the c-axis following the sequence A - [X-T-X] - A - [T-X-T] - A. The $CaBe_2Ge_2$ structure has so far been found less frequently because different atom sizes can not be matched as well as for $ThCr_2Si_2$ [12]. An important example for the $CaBe_2Ge_2$ structure of immediate relevance to the Al-based compounds addressed in our study is $CePd_2Al_2$ [13].

(iii) The $BaNiSn_3$ (*I4mm*) structure is the only subtype lacking an inversion center. In recent years Ce-systems with a $BaNiSn_3$-type structure have generated great interest, since the discovery of superconductivity in heavy fermion systems such as $CeIrSi_3$, $CeRhSi_3$ [14], and $CeCoGe_3$ [15]. In these systems the superconducting pairing symmetry may be outside traditional classification schemes. Shown in Fig. 2 (d) is the characteristic unit cell, where the stacking sequence of layers A-T-X(1)-X(2)-A-T-X(1)-X(2)-A may be readily seen. The point group of these systems is C_{4v}, lacking a mirror plane.

In the following, a brief overview over the literature on CeTAl$_3$ compounds is given. Key properties reported are summarised in Table 1. The crystal structure has been determined as *I4mm* in $CeAuAl_3$ as well as $CeCuAl_3$ in both poly- and single crystals. For $CeAgAl_3$ no distinction has been possible between *I4mm* and *I4/mmm*, whereas $CePtAl_3$ was reported to adopt a centrosymetric variant *I4/mmm*. Interestingly, $CePdAl_3$ has so far been reported to crystallize in the orthorhombic *Fmm2* structure.

Compared to the textbook examples of 3d magnets, crystal electric fields in 4f compounds are weak. Nevertheless, the crystal fields influence the

	Mag	crystal	space group	$T_{C/N}$ (K)	T_K (K)	γ (mJ/molK^2)	μ_{eff} (μ_B)	μ_{CW} (μ_B)
$CeCuAl_3$	AFM	pc, sc	*I4mm* [16, 17, 18]	2.1 [19, 20]	8 [19]	140 [19]	1.8 [17]	2.61 [19]
$CeAgAl_3$	FM	pc	*I4/mmm* or *I4mm* [21]	3.2 [21]	-	-	-	2.23 [21]
$CeAuAl_3$	AFM	pc	*I4mm* [22, 23, 24]	1.32 [23]	4.5 [23]	227 [23]	2.1 [17]	2.6 - 2.8 [24]
$CePdAl_3$	AFM	pc	*Fmm2* [25]	6 [25]	-	-	-	-
$CePtAl_3$	SG	pc	*I4/mmm* [17, 26]	0.8 [26, 25]	-	-	1.8 [17]	2.08 [26]

Table 1: Resume of $CeTAl_3$ properties in literature. AFM - antiferromagnetism, FM - ferromagnetism, SG - Spin-Glass; pc - polycrysal, sc - singlecrystal; $T_{C/N}$ - Curie/Neel-temperature, T_K - Kondo-temperature; μ_{eff} - effective moment, μ_{CW} - Curie-Weiss moment

magnetic properties of 4f systems rather strongly. By Hund's rule, Ce^{3+} has a six-fold degenerate ground state, split into three Kramers doublets by the tetragonal crystal field. In $CeCuAl_3$ it has been reported that the crystal fields are $\Delta_1 = 15\,K$ and $\Delta_2 = 238\,K$ [19, 27]. Further for $CeAuAl_3$ excited levels of $\Delta_1 = 57\,K$ and $\Delta_2 = 265\,K$ [23] as well as $\Delta_1 = 60\,K$ and $\Delta_2 = 240\,K$ [24] have been reported.

Magnetic ground states reported for $CeTX_3$ compounds are typically antiferromagnetic, as in $CeCuAl_3$ with $T_N = 2.1\,K$ and $CeAuAl_3$ with $T_N = 1.32\,K$. However, the exact magnetic ground states reported are incommensuratety modulated, with a propagation vector $\mathbf{k} = (0.4,\ 0.6,\ 0)$ in the case of $CeCuAl_3$ [28] and $\mathbf{k} = (0,\ 0,\ 0.52)$ for $CeAuAl_3$ [29]. In contrast, $CeAgAl_3$ has been reported to represent a rare example of a ferromagnetic Ce-compound with an ordering temperature of $T_C = 3.2\,K$. Last but not least, $CePdAl_3$ has been reported to order antiferromagnetically below 6 K, whereas polycrystalline $CePtAl_3$ has been reported to display spin-glass behaviour below 0.8 K.

All magnetic compounds are characterized by an easy *ab*-plane and a magnetically hard *c*-axes. Kondo temperatures have been determined in $CeCuAl_3$ at 8 K and in $CeAuAl_3$ at 4.5 K, where a weak screening of less than 25 % has been found in an ^{27}Al-NMR study [30]. Both compounds show a heavy fermion ground state, as inferred from an electronic contribution to the specific heat of $\gamma = 227\,mJ/molK^2$ as well as a large prefactor of quadratic temperature dependence of the electric resistivity of $A = 5.0\,\mu\Omega cm/K^2$ in $CeAuAl_3$ [23] and $\gamma = 140\,mJ/molK^2$ in $CeCuAl_3$. Under pressure, T_N has been reported to rise up to 60 kbar in $CeCuAl_3$ suddenly vanishing above 80 kbar [31, 32], putatively pointing towards the existence of a quantum critical point (QCP). Further, recently, a phonon - crystal field quasibound state referred to as vibron has been reported in $CeCuAl_3$ [1], which appears to be absent in $CeAuAl_3$ [29]. Likewise, an anomalous low energy excitation [33] and phonon scattering by Ce magnetic moment fluctuations have been reported in $CeAuAl_3$ [34], as well as a possible second phase transition at 0.18 K [29].

2. Experimental Methods

The physical properties of rare earth containing compounds tend to be very sensitive to defects and impurities. In turn, we have made great efforts to reduce the formation of such defects and contamination by impurities to the lowest possible level. Notably, the procedure of the single-crystal preparation is based on the use of high-purity starting elements and a bespoke work-flow that is optimised to minimise contamination by oxygen, nitrogen and hydro-carbons. As the perhaps most important aspect, we have used optical float-zoning (OFZ) representing a crucible-free technique.

Metal lumps of Ce (Ames, 99.9995%), Au and Ag shot (AlfaAesar Premion, 99.995% 99.9999%), copper lumps (MaTecK, 99.9999%), Pd and Pt powder (AlfaAesar Premion, both 99.995%) and Al lump (MaTecK, 99.9999%) were used for the preparation of the feed and seed rods. Ce and Al were weighted in an argon glove box system. First $CeAl_2$ was prepared in an induction heated horizontal copper cold boat system that can be loaded by means of a bespoke load-lock from a glove box [35]. This reduces contamination of the Ce with oxygen, as the educt $CeAl_2$ is stable on air. In a second step, the $CeAl_2$ was then reacted with the transition metals $T = Cu, Ag, Au, Pd$ or Pt and additional Al in

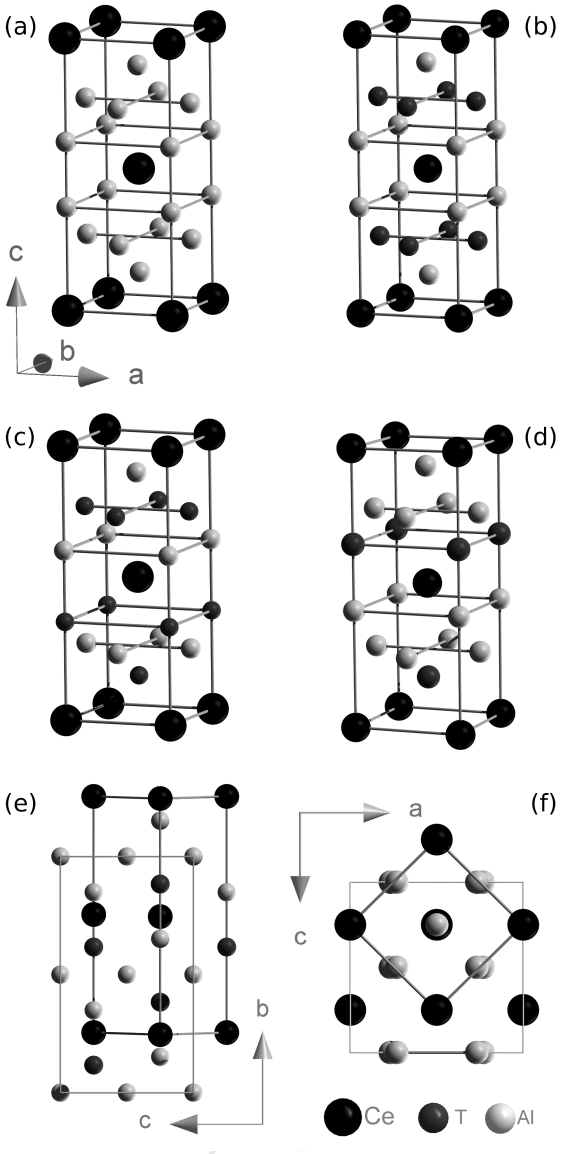

Figure 2: Overview over the $BaAl_4$ parent structure and important subtypes derived of this structure. (a) $BaAl_4$ with space group *I4/mmm* and full inversion symmetry. (b) $ThCr_2Si_2$ with space group *I4/mmm* and full inversion symmetry. (c) $CaBe_2Ge_2$ with space group *P4/nmm* and full inversion symmetry. (d) $BaNiSn_3$ with space group *I4mm*, lacking inversion symmetry. (e) and (f) Schematic representation of the $BaNiSn_3$ structure type and the Cmcm ($PbSbO_2Cl$) structure type.

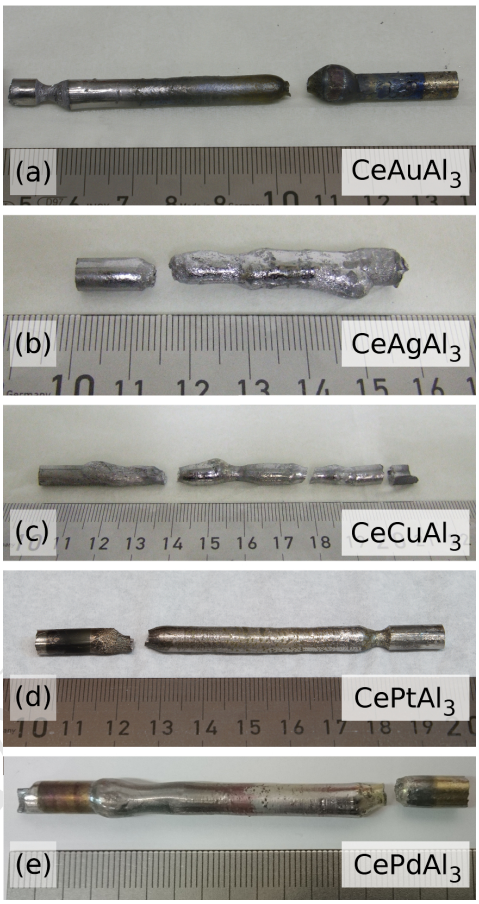

Figure 3: Photographs of all specimen grown by optical float zoning for this study. Scale in cm. (a) $CeAuAl_3$ (b) $CeAgAl_3$ (c) $CeCuAl_3$ (d) $CePtAl_3$ (e) $CePdAl_3$

a water cooled Hukin-type radio frequency heated copper crucible.

The polycrystalline samples were remelted and flipped over several times to ensure good homogeneity. The resulting pellets were subsequently cast into cylindrical feed and seed rods with a diameter of 6 mm and a length of 40 to 60 mm's. Furthermore, synthesis of a polycrystalline sample of $CeNiAl_3$ was attempted by means of our rod casting furnace. For $CeAuAl_3$ the ternary compound was prepared without the intermediate step of first synthesising $CeAl_2$ by means of the glove box and the horizontal cold boat system and the bespoke load-lock.

The actual single crystal growth was performed in a CSI 4-mirror (model FZ-T 10000-H-III-VPS) optical float zone furnace. The furnace was redesigned to be all-metal sealed. Prior to growth

the furnace was baked with bespoke heating jackets [36]. 500 W halogen lamps were used for the growth process under a static argon atmosphere at a pressure of 2.5 bar. The float zoning was performed with a growth rate of 5 mm/h and a counter rotation of 6 rpm of the feed and seed rod, respectively.

The characterization of the crystals proceeded as follows. First, all crystals were examined under an optical light microscope. Laue X-ray (Multiwire Laboratories MWL 110) images were taken on different spots covering all of the surface of the ingot to identify the single crystalline part and possible grain boundaries. In $CeAuAl_3$ additionally cross sections of the upper and lower part of the crystal were analysed as well as a cut through the quenched final part of the molten zone. Figure 1 (a) shows from right to left the polycrystalline feed rod, the quenched molten zone with a pronounced stripe structure and the beginning of the single crystal at the lower end.

All crystals were oriented by Laue X-ray diffraction. Fig. 1 (b) and (c) show typical Laue pictures of $CeAuAl_3$ for the *a*- and *c*-axes, respectively. The composition was confirmed by single crystal and powder X-ray diffraction. For $CeAuAl_3$ additional scanning electron microscope images and energy dispersive X-ray spectra were recorded.

Small single crystals with dimensions less than 100 μm were mechanically extracted from $CeTAl_3$ (T = Cu, Ag, Au, Pd and Pt) ingots as grown. Generally all tested crystals were of high quality with sharp diffraction peaks. Intensity data were collected with graphite-monochromatized Mo Kα X-ray radiation. Three-dimensional data were indexed, integrated and corrected for Lorentz-, polarization, absorption and background effects using a diffractometer specific software, namely CrystalClear for a Rigaku Saturn724+ and X-Area for a STOE IPDS II. Initial structure analysis/solution (using direct methods) for $CeTAl_3$ (T = Cu, Ag, Au, Pt) was done with SHELX-2012 as implemented in the program suite WinGX 2014.1 [37]. The crystal structure of modulated $CePdAl_3$ was solved using WinCSD [38].The experimental data and results of the structure refinement for selected samples are reported in Table 3, while the fractional atomic coordinates, occupation numbers and equivalent isotropic, and anisotropic atomic displacement parameters are listed in Table 4 and 5.

Samples for resistivity measurements were cut from the single-crystalline sections of the ingots with a diamond wire saw. Typical dimension of the samples were between 4 and 6 $\times$ 1 $\times$ 0.2 mm^3, oriented such that the electrical current could be applied along longest direction which corresponding to the *c*-axis. The resistivity was measured in a standard four-probe ac-configuration using a digital lock-in amplifier and an excitation current of 5 mA at an excitation frequency of 22.08 Hz. Room temperature transformers were used for impedance matching. Data were recorded between 2 K and 300 K in a standard ^{4}He cryostat. Data down to much lower temperatures were measured for $CeTAl_3$ with T = Cu, Ag, Au in an adiabatic demagnetisation refrigerator (ADR) using the same detection technique at a lower excitation current of 1 mA down to a temperature below $\sim$300 mK. For samples with T = Pt, Pd a ^{3}He/^{4}He dilution refrigerator was used down to temperatures well below 100 mK.

3. Experimental Results

3.1. Crystal Structure

The actual growth process resulted in the specimens shown in Fig. 3. We obtained large single crystals of $CeAuAl_3$, $CeCuAl_3$ and $CePtAl_3$ shown in Figs. 3 (a), (c) and (d), respectively. While these ingots remained mechanically intact after growth, the $CeCuAl_3$ ingot (shown in Fig. 3 (a)) fractured spontaneously in one location after cool-down. For $CeAgAl_3$ single crystalline grains were prepared from the specimen. The molten zone in the growth process of $CePdAl_3$ was very unstable and we could only prepare small single crystalline samples with a typical size of up to 3 mm. A second attempt to grow $CePdAl_3$ with a reduced growth rate of 1 mm/h allowed to obtain the large single crystal depicted in Fig. 3 (e). Note that all measurements on $CePdAl_3$ reported in this paper were carried out on samples cut from the first crystal.

Additionally a weighted-in quantity of $CeNiAl_3$ was synthesized in the Hukin-type cold crucible. The resulting pellet was analysed by powder X-ray diffraction and revealed a composition $CeNi_2Al_5$ with $CeAl_2$ and $CeNi_2Al_3$, where small single crystals were extracted.

The analysis of the arrays of the diffraction data revealed that the majority of the $CeTAl_3$ compounds (T = Cu, Au, Pt) studied display reflections consistent with the tetragonal lattice and in line with one of the distorted $BaAl_4$ structure types. The T/Al antisite disorder essentially corresponds to the local differences between $ThCr_2Si_2$,

$CaBe_2Ge_2$, $HoCuAl_3$ or $BaNiSn_3$ structures. Extinction of characteristic reflections revealed a body centred tetragonal lattice and the structure solution corresponded to a $BaNiSn_3$ type structure for $CeAuAl_3$, $CeCuAl_3$ and $CePtAl_3$. The evidence for putative Au/Al antisite disorder in $CeAuAl_3$ was below the detection limit, whereas for $CeCuAl_3$ a small Cu/Al mixing on the copper site was observed consistent with a ∼5 % site occupation factor (sof) deficiency on the 4*b* Al site. A higher degree of antisite disorder was found in the $CePtAl_3$ sample. Assuming a stoichiometric composition and fully occupied atomic sites of $CePtAl_3$, the antisite Pt/Al disorder appeared to be as high as 18 % sof at both T and Al 2*a* sites. The obtained unit cell volumes were found to decrease in the series Au – Pt – Cu in accordance with the metallic radii ($r_{\mathrm{Au}} = 1.44$ Å, $r_{\mathrm{Pt}} = 1.39$ Å, $r_{\mathrm{Cu}} = 1.28$ Å) [39].

For $CeAgAl_3$ a small orthorhombic distortion of the $BaAl_4$ type lattice of the order of ∼ 0.1 Å was detected. The character of the splitting of the reflection and the extinction revealed a *C*-base centred orthorhombic lattice with $a_0 \approx a_T\sqrt{2}$, $b_0 \approx c_T$ and $c_0 \approx a_T\sqrt{2}$, where *O* and *T* denote orthorhombic and tetragonal lattice dimensions. The structure solution leads to the *Cmcm* space group and a model consistent with the structure type of $PbSbO_2Cl$. The orthorhombic superstructure observed occurs in oxyhalides and is found rarely in intermetallics, e.g., in $LaZn_4$ [40] and $SrPdGa_3$ [41, 42]. Similar to $CeCuAl_3$ a small Ag/Al mixing occurs on the Ag site along with a weak (ca. 4 % sof) deficiency on the 8*e* Al site.

A comparison of the Ag and Au based $CeTAl_3$ structures is plotted in Fig. 2 (e) and (f). We note, that Ag and Au nominally possess the same metallic radii ($r_{\mathrm{Ag}} = 1.44$ Å), which may correspond to a similar magnitude of chemical pressure in both $CeTAl_3$ (T = Ag, Au). Indeed, the normalised lattice dimensions of $CeAgAl_3$ ($a_T \approx (a_0+b_0)/2\sqrt{2} \approx 4.3566(8)$ Å, $c_T \approx 10.837(2)$ Å) are very similar to these of $CeAuAl_3$. Further, the relative cerium and aluminium positions reproduce well, whereas major differences were noticed for the distribution of gold and silver sites. By their arrangement the structure may be viewed as an intermediate step between $BaAl_4$ (or $HoCuAl_3$) and the $BaNiSn_3$ structure type. The antisite disorder observed smears out the layered structure along the c-axis in $CeAgAl_3$, which initially can be described as A - [TX-X-TX] A, where TX indicated mixed T and X layer occupation.

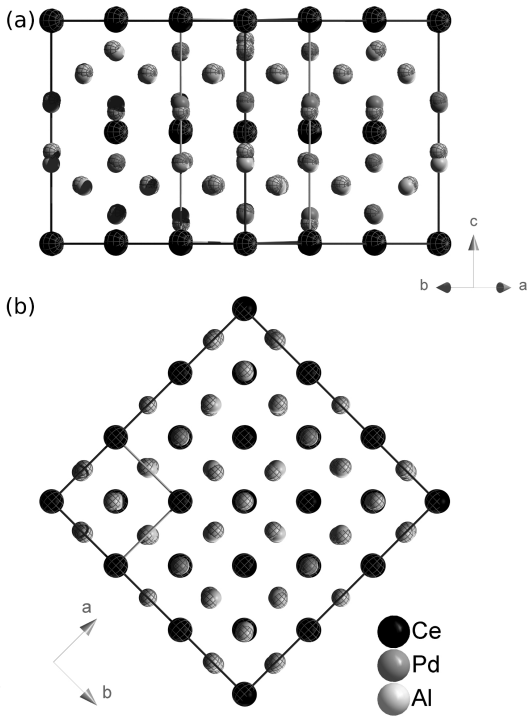

Figure 4: Refined structural modifications of $CePdAl_3$: plane atoms - $BaNiSn_3$ type of structure, structured atoms - *klassengleiche* [43] subgroup of $BaNiSn_3$ type of structure with 3*a* multiplied axis.

This brings us to $CePdAl_3$ for which the full structure determination was performed on a small single crystal. The set of Bragg reflections collected for the $CePdAl_3$ single crystal could neither be described with a conventional tetragonal nor with orthorhombic lattices. Careful indexing was finally found to be consistent with a tetragonal cell with a *c*-parameter comparable to $CeTAl_3$ (T = Cu, Ag, Au, Pt), however, with an *a* lattice parameter multiplied by a factor of ∼ 3. Analysis of peak systematics resulted in a solution corresponding to a body centred tetragonal lattice. This is in agreement with group theory, as the 3*a*, *c* axis multiplication in the *I4mm* space group is allowed in the frame of *klassengleiche* [43] subgroups IIc for *I4mm* (3*a* structure). Multiplication of the axis implies a splitting of the Ce and Pd positions into three independent sites, whilst the two initial aluminium sites are split into seven positions in the larger cell. Similar to $CeCuAl_3$, $CePtAl_3$, $CeAgAl_3$ Rietveld refinement revealed Pd/Al antisite disorder, where,

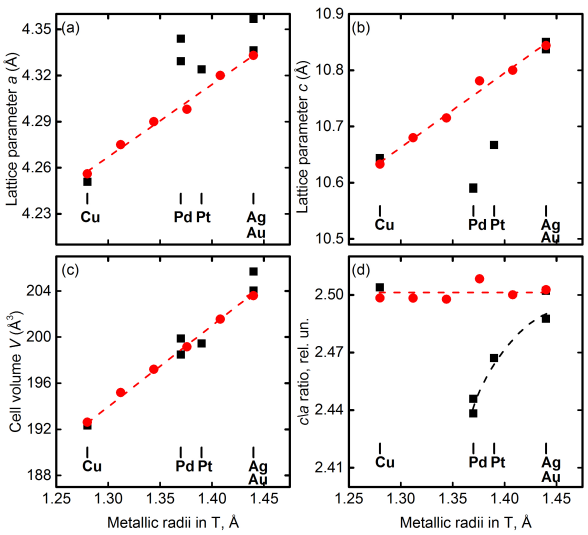

Figure 5: Lattice parameter, cell volume and c/a ratio for different CeTAl$_3$ (T = Cu, Ag, Au, Pd, Pt) plotted as a function of T metallic radius (black squares). Data showed by red circles correspond to CeAu$_{1-x}$Cu$_x$Al$_3$ solid solution taken from [44]. Two data points for CePdAl$_3$ correspond to BaNiSn$_3$ and 3a structures. The lines are showed as guides for the eyes.

however, only one Pd site of three as well as two of the seven Al sites are affected. It is important to emphasize, that the 3a structure was only observed in a small CePdAl$_3$ single crystal, and has so far not been confirmed in powder diffraction as explained in the following.

Examination of a crushed and pulverized ingot using lab X-ray powder diffraction did not reveal any hints for a 3a structure, but a conventional BaNiSn$_3$ modification for CePdAl$_3$ (see Table 5). The crystal structures of both the BaNiSn$_3$-type and the 3a, c axis multiplied modifications of the CePdAl$_3$ structures are shown in Fig. 4. The Ce(0,0,0) atomic position is here used as a reference. In comparison to the BaNiSn$_3$-type modification of CePdAl$_3$, the 3a structure contains a certain degree of Pd/Al disorder and by its layer structure A - [TX-X-TX] - A it becomes very similar to CeAgAl$_3$. An attempt to refine the structure modulation in CePdAl$_3$ was performed assuming both commensurate and incommensurate modulation vectors of the BaNiSn$_3$ parent structure. The atomic modulated displacements were comparable to standard uncertainties of atom localization and improvement to fit residuals (when compared to the structure model with 3a, c axis multiplication), and

	ρ_0 ($\mu\Omega$cm)	RRR	$\rho_{300\,K}$ ($\mu\Omega$cm)
CeCuAl$_3$	12.9	2.84	36.6
CeAgAl$_3$	7.9	3.81	30.1
CeAuAl$_3$	15.2	2.50	37.8
CePdAl$_3$	25.1	1.39	35.0
CePtAl$_3$	67.4	1.25	84.1

Table 2: Parameters derived from resistivity measurements on CeTAl$_3$ with T = Cu, Ag, Au, Pd and Pt. ρ_0 is the residual resistivity extrapolated to T = 0, RRR the residual resistivity ratio $\rho(300\,\mathrm{K})/\rho_0$, where $\rho(300\,\mathrm{K})$ denotes the resistivity at room temperature.

thus, found to be marginal. Taken together this provides strong putative evidence of a 3a structure, requiring further studies to be confirmed.

The lattice parameters of the CeTAl$_3$ (T = Cu, Ag, Au, Pd, Pt) samples studied were found to be in a good agreement with experimental data reported in Refs. [44, 16, 45, 27, 20]. Cell volumes in CeTAl$_3$ (T = Cu, Ag, Au, Pd, Pt) follow a linear dependence as a function of T ionic radii (see Fig. 5) in line with values reported for the CeAuAl$_3$ to CeCuAl$_3$ pseudobinary system [44], which displays a behaviour characteristic of Vegards law. The observed linear dependence may be viewed in terms of structural changes in CeTAl$_3$ (T = Cu, Ag, Au, Pd, Pt) driven by chemical pressure. However, all CeTAl$_3$ studied are characterised by a large anisotropy. Notably, for CeCuAl$_3$, CeAuAl$_3$ and related solid solutions [44] the c/a ratio is nearly constant with $c/a \sim 2.5$. CePdAl$_3$ CePtAl$_3$ and CeAgAl$_3$, display systematically lower c/a values.

For these compounds the experimentally determined a lattice parameters are systematically higher, as well as the c lattice parameters, which are systematically smaller than those observed in the CeAuAl$_3$ – CeCuAl$_3$ pseudobinary series. Taking into account nominally equal metallic radii for Au and Ag, the differences observed for the a lattice dimensions and cell volume of CeAuAl$_3$ and CeAgAl$_3$ as well as their different structure, significantly reduces the relevance of an approximation in the spirit in terms of chemical pressure and shows that the chemical nature of T in CeTAl$_3$ plays a dominant role for the structure and its distortion.

3.2. Electrical Resistivity

Shown in Fig. 6 (a1) to (a5) is the electric resistivity for CeTAl$_3$ with T = Cu, Ag, Au, Pd and Pt covering three decades of temperature from $\sim$ 0.1 K to 300 K. For these data the electrical currents were

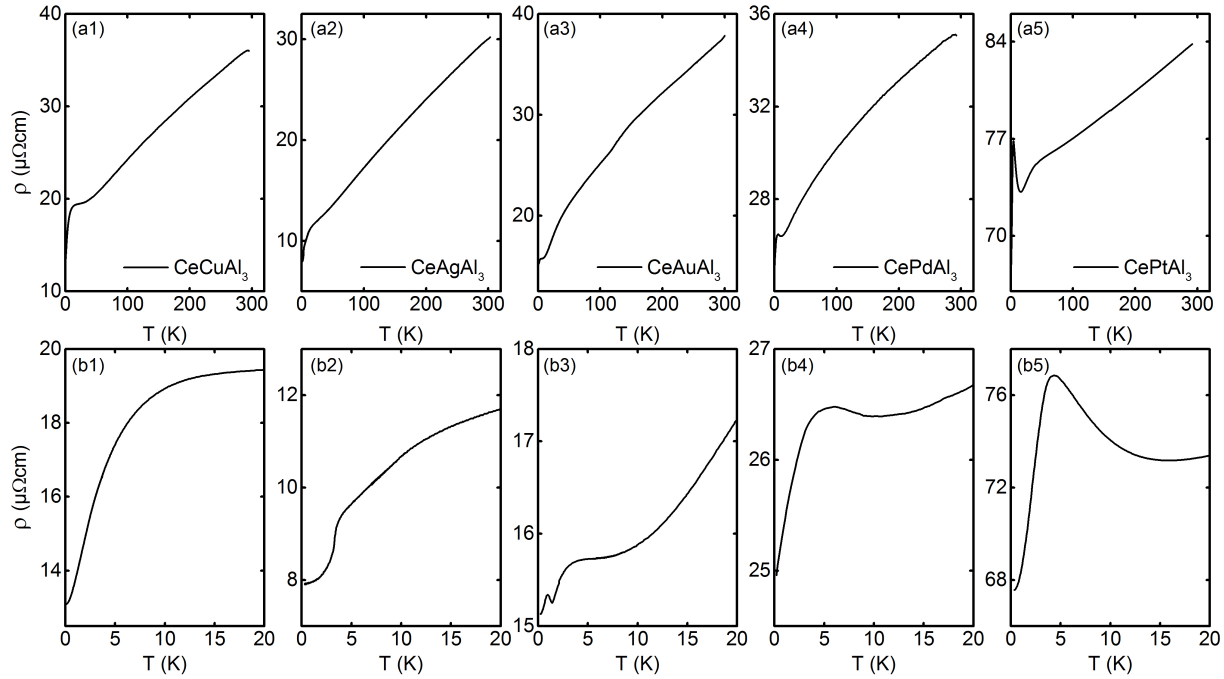

Figure 6: Electrical resistivity for CeTAl$_3$ with T = Cu, Ag, Au, Pd, Pt. (a1) - (a5) On a large temperature range from T_{min} = 300 mK to 300 K all samples show metallic behaviour. (b1) - (b2). Close-up view of the behaviour at low temperatures up to 20 K.

applied parallel to the crystallographic c-axis. Further, Fig. 6 (b1) - (b5) shows the same data on a temperature scale up to 20 K for a better visibility of the low temperature features.

All samples show metallic behaviour over the complete temperature range. The residual resistivity, resistivity at 300 K and associated residual resistivity ratios (RRR) of all compounds are summarized in Table 2. The residual resistivity ρ_0 for all compounds are among the best reported in literature. The values of the RRR observed are lower than for Si or Ge based compounds, probably due to the remaining antisite disorder in our samples. We wish to note that preliminary work suggests, that careful annealing studies and tiny adjustments to the starting compositions as well as variations of the parameters used for single crystal growth promise considerable improvements as compared to the values observed here.

The key features observed in the temperature dependences may be summarised as follows. In $CeCuAl_3$ the linear decrease at high temperatures is followed by a plateau between 30 K and 10 K, whereas a clear maximum as reported in Refs. [20, 28] is not observed. The strong decrease below 10 K traditionally is attributed to the coherence of a Kondo lattice, where a clear signature of the magnetic ordering transition at 2.1 K is not observed and maybe hidden by this Kondo coherence. However, on a speculative note an alternative scenario may be related to the strong electron-phonon interactions associated with the quasi-bound vibron. Below 0.5 K the decrease flattens towards a residual resistivity of 12.9 $\mu\Omega$cm, which is among the lowest reported in the literature for this compound.

A linear decrease is observed in $CeAgAl_3$ down to approximately 17 K, followed by a steeper linear decrease. The change of slope is of unknown origin, but may be due to the changes of the coupling with the lattice degrees of freedom. Such a strong coupling of a crystal electric field (CEF) with a phonon is discussed in $CeCuAl_3$ [1] and $CePd_2Al_2$ [46]. A clear kink at 3.2 K, corresponding to the magnetic transition temperature of ferromagnetic order reported in the literature, is followed by a quadratic temperature dependence down to the lowest temperatures. The specific temperature dependence may be characteristic of weakly spin-

polarised Fermi liquid, in which electron magnon scattering is weak.

For $CeAuAl_3$ the resistivity decreases from 300 K to 15 K in a quasi-linear manner, probably due to crystal electric field effects as discussed in Ref. [23]. With decreasing temperature the decrease of the resistivity is followed by a plateau around 8 K and another strong decrease below the onset of magnetic order at 1.32 K. However the onset of the decrease at 4.5 K is considerably higher than T_c and maybe attributed to the coherence of a Kondo lattice. At ∼1 K, an additional maximum due to the opening of a super-zone gap is observed reminiscent of behaviour observed in CeGe [47] and Cr [48].

$CePdAl_3$ shows a sublinear decrease over the entire temperature range, probably due to crystal field effects. A faint maximum is visible around 5.7 K, again attributed to the onset of the Kondo effect, and followed by a strong decrease down to the lowest temperatures, most probably caused by Kondo coherence. Towards the lowest temperatures there is a linear decrease of the resistivity instead of a flattening out. We do not observe any features suggesting magnetic order over the whole temperature range, suggested to exist below 6 K in the literature.

Last but not least, the linear decrease of the resistivity in $CePtAl_3$ down to ∼ 50 K is followed by a stronger decrease to a minimum at 15.9 K. The origin of this kink may be again, as speculated above, related to changes of the coupling to the crystal lattice. An exponential increase to a maximum at 4.3 K is most probably due the onset of Kondo scattering and followed by a strong decrease consistent with Kondo coherence. Towards the lowest temperatures, the decrease flattens and is extrapolated to a residual resistivity of 25.1 $\mu\Omega$cm. Overall, the resistivity is about a factor of three higher than for other compounds studied, which may be due to the higher degree of antisite disorder. There are no signs suggesting magnetic order, however below ∼0.8 K the decrease of the resistivity flattens out.

4. Conclusions

Single crystals of the non-centrosymmetric intermetallic compounds $CeTAl_3$ (T = Cu, Ag, Au, Pd and Pt) were grown by means of optical float-zoning, to the best of our knowledge for the first time. Large single crystals were obtained for all compounds except $CeAgAl_3$. For $CePdAl_3$ the growth rate had to be reduced from 5 mm/h to 1 mm/h to be stable. An attempt to grow a polycrystal of $CeNiAl_3$ resulted in a mixture dominated by $CeNi_2Al_5$. The crystal structure of the parent compounds was determined by single crystal X-ray diffraction. The crystal structure was found to be $BaNiSn_3$-type *I4mm* in all cases except for $CeAgAl_3$, which shows a small distortion corresponding to the orthorhombic *Cmcm* structure. Further, we find strong putative evidence that the space group of $CePdAl_3$ has a three fold multiplied lattice parameter a, which is allowed by group theory. Although the unit cell volume for all systems follows the metallic radii of the transition metal element rather well, the c/a ratio is deviating strongly.

Site-antisite disorder of the T and X-site appears to be nominally absent in $CeAuAl_3$, but reaches a value as high as 18 % in $CePtAl_3$, nominally explaining the larger residual resistivities as compared to the Si and Ge based compounds in this series. While the sample quality of our samples as grown is already high, we expect that careful studies addressing the precise growth conditions and the role of post-growth treatment, such as annealing and/or electro-transport, promise significant improvements.

Further, resistivity measurements as described in the traditional language used for Ce-based compounds are consistent with Kondo behaviour for all samples except $CeAgAl_3$. The occurrence of the Kondo maximum depends thereby on the transition metal element and is most pronounced for T = Pt. It is interesting to speculate, if, what seems to be Kondo-like behaviour, eventually turns out to be due to strong electron-phonon coupling as related to the notion of the quasi-bound vibron state reported in $CeCuAl_3$. As a final point, features in the resistivity of $CeAuAl_3$, $CeCuAl_3$ and $CeAgAl_3$ at low temperatures are consistent with published reports of antiferromagnetic order in the former two compounds and ferromagnetism in the latter system, respectively. This contrasts the literature on $CePtAl_3$ and $CePdAl_3$, where we do not find signs of magnetic order down to 0.1 K in the resistivity, whereas spin glass order has been reported for polycrystalline $CePtAl_3$ and antiferromagnetic order for $CePdAl_3$.

Taken together all single-crystals are of high quality consistent with very low residual resistivities as compared to the literature. This demonstrates that optical float-zoning as employed under pure conditions provides an excellent method for the preparation of Ce-based intermetallic compounds.

5. Acknowledgements

We wish to thank Matthias Ruderer for access to the glove box of E13, Rainer Jungwirth (FRMII) for EDX measurements on $CeAuAl_3$, the TUM crystal laboratory for orienting with Laue X-ray diffraction and cutting and polishing of the samples. Financial support of the Deutsche Forschungsgemeinsschaft and DFG TRR80 are gratefully acknowledged.

References

[1] D. T. Adroja, A. del Moral, C. de la Fuente, A. Fraile, E. A. Goremychkin, J. W. Taylor, A. D. Hillier, F. Fernandez-Alonso, Vibron Quasibound State in the Noncentrosymmetric Tetragonal Heavy-Fermion Compound $CeCuAl_3$, Phys. Rev. Lett. 108 (2012) 216402.

[2] M. Loewenhaupt, B. D. Rainford, F. Steglich, Dynamic Jahn-Teller Effect in a Rare-Earth Compound: $CeAl_2$, Phys. Rev. Lett. 42 (1979) 1709–1712.

[3] P. Thalmeier, P. Fulde, Bound State between a Crystal-Field Excitation and a Phonon in $CeAl_2$, Phys. Rev. Lett. 49 (1982) 1588–1591.

[4] D. Souptel, G. Behr, W. Löser, A. Teresiak, S. Drotziger, C. Pfleiderer, $CeSi_{2-\sigma}$ single crystals: growth features and properties , J. Cryst. Growth 269 (2-4) (2004) 606 – 616.

[5] C. Cao, M. Deppe, G. Behr, W. Löser, N. Wizent, O. Kataeva, B. Büchner, Single Crystal Growth of the $CeCu_2Si_2$ Intermetallic Compound by a Vertical Floating Zone Method, Cryst. Growth Des. 11 (2) (2011) 431–435.

[6] C. Bergmann, H. S. Jeevan, M. Schubert, C. Geibel, P. Gegenwart, Single crystal growth of $CeNi_2Ge_2$ using the floating zone technique, Phys Status Solidi B 247 (3) (2010) 694–696.

[7] M. Edwards, S. Horn, R. Parks, Effects of crystal fields on the scaling behavior of the magnetic susceptibility in $Ce(Ni_xCu_{1-x})_2Si_2$, Solid State Commun. 61 (1) (1987) 65 – 69.

[8] F. de Boer, J. Klaasse, P. Veenhuizen, A. Böhm, C. Bredl, U. Gottwick, H. Mayer, L. Pawlak, U. Rauchschwalbe, H. Spille, F. Steglich, $CeCu_2Ge_2$: Magnetic order in a Kondo lattice, J. Magn. Magn. Mater. 63 (1987) 91 – 94.

[9] R. Ballestracci, G. Astier, Etude cristallographique des siliciures ternaires de terres rares, MRu_2Si_2 et MPt_2Si_2, C. R. Acad. Sci. Ser. B (286) (1978) 109–112.

[10] G. Cordier, E. Czech, H. Schäfer, P. Woll, Structural characterization of new ternary compounds of uranium and cerium, J Less-Common Met. 110 (1) (1985) 327 – 330.

[11] M. Rotter, M. Tegel, D. Johrendt, I. Schellenberg, W. Hermes, R. Pöttgen, Spin-density-wave anomaly at 140 K in the ternary iron arsenide $BaFe_2As_2$, Phys. Rev. B 78 (2) (2008) 020503.

[12] L. Frik, D. Johrendt, A. Mewis, Eine neue Verzerrungsvariante des $CaBe_2Ge_2$-Typs–Die Kristallstrukturen von $SrPd_2Bi_2$, $BaPd_2Bi_2$ und $BaAu_2Sb_2$, Z. Anorg. Allg. Chem. 632 (8-9) (2006) 1514–1517.

[13] M. Klicpera, P. Javorský, A. Hoser, Structural and electronic properties of $RPd_2Al_{2-x}Ga_x$ (R = Ce and La) compounds, J. Alloy. Compd. 596 (2014) 167–172.

[14] W. Xian-Zhong, L. B., W. L. Ng, C. B., E. J., H. P., Aspects cristallochimiques et existence des siliciures ternaires $MTSi_3$ de structure type $BaNiSn_3$ (M=Th, Y, Ln et T=Ru, Os, Co, Rh, Ir), Rev. Chim. Miner. 22 (6), francais.

[15] A. Das, R. Kremer, R. Pöttgen, B. Ouladdiaf, Magnetic ordering in $CeCoGe_3$, Physica B 378-380 (2006) 837 – 838.

[16] O. Moze, K. Buschow, Crystal structure of $CeCuAl_3$ and its influence on magnetic properties, J. Alloy. Compd. 245 (1-2) (1996) 112 – 115.

[17] S. Mock, C. Pfleiderer, H. v. Löhneysen, Low-Temperature Properties of $CeTAl_3$; (T=Au, Cu, Pt) and $CeAuGa_3$;, J. Low. Temp. Phys. 115 (1999) 1–14.

[18] M. Klicpera, P. Javorský, P. Čermák, A. Rudajevová, S. Daniš, T. Brunátová, I. Císařová, Crystal structure and its stability in $CeCuAl_3$ single crystal, Intermetallics 46 (2014) 126 – 130.

[19] E. Bauer, N. Pillmayr, E. Gratz, G. Hilscher, D. Gignoux, D. Schmitt, On the behaviour of the new Kondo lattice $CeCuAl_3$, Z. Phys. B Con. Mat. 67 (1987) 205–210.

[20] M. Kontani, H. Ido, H. Ando, T. Nihioka, Y. Yamaguchi, Magnetic, Transport and Thermal Properties of $CeCuAl_3$ Single Crystal, J. Phys. Soc. Jpn. 63 (5) (1994) 1652–1655.

[21] T. Muranaka, J. Akimitsu, Thermodynamic properties of ferromagnetic Ce-compound, $CeAgAl_3$, Physica C 460-462, Part 1 (0) (2007) 688 – 690.

[22] F. Hulliger, On new rare earth gold aluminides LnAuAl, J. Alloy. Compd. 200 (1-2) (1993) 75 – 78.

[23] S. Paschen, E. Felder, H. Ott, Transport and thermodynamic properties of $CeAuAl_3$, Eur. Phys. J. B 2 (2) (1998) 169–176.

[24] H. Sugawara, S. Saha, T. Matsuda, Y. Aoki, H. Sato, J. Gavilano, H. Ott, Magnetic and transport properties in $CeAuAl_3$ single crystal, Physica B 259-261 (0) (1999) 16 – 17.

[25] C. Schank, F. Jährling, L. Luo, A. Grauel, C. Wassilew, R. Borth, G. Olesch, C. Bredl, C. Geibel, F. Steglich, 4f-conduction electron hybridization in ternary CeTMAl compounds, J. Alloy. Compd. 207-208 (0) (1994) 329 – 332.

[26] T. Görlach, Tieftemperatureigenschaften der intermetallischen Ce- und Yb-Verbindungen $CePtAl_3$, $La_{1-x}Ce_xCu_6$, $YbAl_2$ und $YbPd_{1-x}Pt_xSn$, Ph.D. thesis, Univ. Göttingen (2006).

[27] S. A. M. Mentink, N. M. Bos, B. J. van Rossum, G. J. Nieuwenhuys, J. A. Mydosh, K. H. J. Buschow, Antiferromagnetism and crystalfield effects in $CeCuX_3$ (X=Al,Ga) compounds, J. Appl. Phys. (10) (1993) 6625 –6627.

[28] M. Klicpera, P. Javorskỳ, M. Diviš, Magnetization and electrical resistivity measurements on $CeCuAl_3$ single crystal, J. Phys.: Conf. Ser. 592, IOP Publishing, 2015, p. 012014.

[29] D. T. Adroja, C. de la Fuente, A. Fraile, A. D. Hillier, A. Daoud-Aladine, W. Kockelmann, J. W. Taylor, M. M. Koza, E. Burzurí, F. Luis, J. I. Arnaudas, A. del Moral, Muon spin rotation and neutron scattering study of the noncentrosymmetric tetragonal compound $CeAuAl_3$, Phys. Rev. B 91 (2015) 134425.

[30] P. Vonlanthen, J. Gavilano, B. Ambrosini, H. Ott, ^{27}Al nuclear magnetic resonance studies of $CeAuAl_3$, Physica B 259-261 (1999) 18 – 19.

[31] Y. Kawamura, T. Nishioka, H. Kato, M. Matsumura, K. Matsubayashi, Y. Uwatoko, High pressure electrical resistivity of $CeCuAl_3$, J. Phys.: Conf. Ser. 200 (1) (2010) 012082.
[32] T. Nishioka, Y. Kawamura, H. Kato, M. Matsumura, K. Kodama, N. Sato, High pressure magnetization measurements of $BaNiSn_3$-type $CeCuAl_3$, J. Magn. Magn. Mater. 310 (2, Part 1) (2007) e12 – e14.
[33] Y. Aoki, M. A. Chernikov, H. R. Ott, H. Sugawara, H. Sato, Thermal conductivity of $CeAuAl_3$: Evidence of phonon scattering by Ce magnetic moment fluctuations, Phys. Rev. B 62 (2000) 87–90.
[34] Y. Aoki, S. Saha, T. Matsuda, H. Sugawara, H. Sato, Anomalous low-energy excitation in $CeAuAl_3$, Physica B 281-282 (0) (2000) 110 – 111.
[35] A. Bauer, A. Neubauer, W. Münzer, A. Regnat, G. Benka, M. Meven, B. Pedersen, C. Pfleiderer, Ultra-high vacuum compatible induction-heated rod casting furnace, Rev. Sci. Inst. 87 (2016) 063909.
[36] A. Neubauer, J. Boeuf, A. Bauer, B. Russ, H. v. Löhneysen, C. Pfleiderer, Ultra-high vacuum compatible image furnace, Rev. Sci. Inst. 82 (1) (2011) 013902.
[37] L. J. Farrugia, *WinGX* and *ORTEP for Windows*: an update, J. Appl. Crystallogr. 45 (4) (2012) 849–854.
[38] L. Akselrud, Y. Grin, WinCSD: software package for crystallographic calculations (Version 4), J. Appl. Crystallogr. 47 (2014) 803–805.
[39] N.N.Greenwood, A. Earnshaw, Chemistry of the Elements, Butterworth-Heinemann, 1997.
[40] I. Oshchapovsky, V. Pavlyuk, A. Dmytriv, G.and Griffin, Lanthanum tetrazinc, $LaZn_4$, Acta Crystallogr. C 68 (6) (2012) i37–i40.
[41] S. Seidel, R. D. Hoffmann, R. Pöttgen, $SrPdGa_3$ - An orthorhombic superstructure of the $ThCr_2Si_2$ type, Z. Kristallogr. 229 (6) (2014) 421–426.
[42] S. Seidel, O. Niehaus, S. F. Matar, O. Janka, B. Gerke, U. C. Rodewald, R. Pöttgen, The gallium intermetallics $REPdGa_3$ (RE = La, Ce, Pr, Nd, Sm, Eu) with $SrPdGa_3$-type structure, Z. Naturforsch. B 69 (11-12) (2014) 1105–1118.
[43] According to the International Tables for Crystallography (Vol. A, 2.2.15.1), the The maximal non-isomorphic subgroups of a space group are divided into two types: (I) so-called *translationengleiche* or t subgroups, and (II) *klassengleiche* or k subgroups.
[44] M. Klicpera, P. Javorský, Study of electronic properties in $RCuAu_xAl_3$ compounds, where R=Ce, La, J. Magn. Magn. Mater. 363 (2014) 88–94.
[45] O. S. Zarechnyuk, P. Kripyakevich, E. Gladyshevskij, Ternary Intermetallic Compounds with a $BaAl_4$ Type Superlattice, Sov. Phys. Crystallogr 9, translated from Kristallografiya, 9, 835-838 (1964).
[46] L. Chapon, E. Goremychkin, R. Osborn, B. Rainford, S. Short, Magnetic and structural instabilities in $CePd_2Al_2$ and $LaPd_2Al_2$, Physica B 378-380 (2006) 819 – 820.
[47] P. K. Das, N. Kumar, R. Kulkarni, S. K. Dhar, A. Thamizhavel, Anisotropic magnetic properties and superzone gap formation in CeGe single crystal, J. Phys. Condens. Mat. 24 (14) (2012) 146003.
[48] B. Stebler, The Resistivity Anomaly in Chromium Near the Neel Temperature, Phys. Scripta 2 (1-2) (1970) 53.

	$CeAgAl_3$	$CeAuAl_3$	$CeCuAl_3$	$CePdAl_3$	$CePtAl_3$
Diffractometer	Stoe IPDS-II	Rigaku Saturn724+	Stoe IPDS-II	Stoe IPDS-II	Rigaku Saturn724+
Radiation		MoKα			
Wavelength (Å)		0.71073			
Abs. correction type		empirical			
Abs. coeff. μ	15.737	237.31	16.792	161.11	232.91
Crystal system	Orthorhombic	Tetragonal	Tetragonal	Tetragonal	Tetragonal
space group	Cmcm	I4mm	I4mm	I4mm	I4mm
a (Å)	6.205(1)	4.3364(4)	4.2508(4)	12.988(1)	4.3239(4)
b (Å)	10.837(2)	4.3364(4)	4.2508(4)	12.988(1)	4.3239(4)
c (Å)	6.118(1)	10.850(2)	10.644(1)	10.589(1)	10.667(2)
V (Å^3)	411.4(1)	204.03(4)	192.32(3)	1786.2(5)	199.43(4)
Z	4	2	2		2
ρ_{calc} (g/cm^3)	5.206	6.805	4.758	5.421	6.930
index range h	-9...9	-5...6	-5...5	-17...17	-6...3
	-16...16	-3...6	-5...5	-17...17	-6...5
	-9...8	-16...14	-14...14	-14...14	-16...16
reflections collected	14323	1821	2475	6685	879
independent reflections	417	226	100	703	141
R_{int} (%)	9.52	3.52	10.49	2.00	3.45
RF2 (%)	6.61	5.25	2.18	8.21	7.60
RF2w (%)	5.45	9.36	5.79	6.29	8.50
RF (%)	3.30	3.78	2.00	5.84	4.81
χ^2	0.369	1.98	1.373	5.84	2.24
no. of free parameters	19	14	14	26	14

Table 3: Experimental details and results of the structure refinement of CeTAl$_3$ (T = Cu, Ag, Au, Pd, Pt) as studied at ambient conditions.

Atom	Wyckoff	x/a	y/b	z/c	sof	u_{eq}	u_{11}	u_{22}	u_{33}	u_{12}	u_{13}	u_{23}
$CeAgAl_3$, space group *Cmcm*, a = 6.2050(12) Å, b = 10.837(2) Å, c = 6.118(1) Å												
Ce	4c	0	0.24552(6)	1/4	1.0	0.0105(4)	0.0097(3)	0.0102(3)	0.0117(5)	0	0	0
Ag1	4c	1/2	0.38336(9)	1/4	0.918(8)	0.0133(5)	0.0125(4)	0.0123(5)	0.0150(6)	0	0	0
Al1	4c	1/2	0.38336(9)	1/4	0.082(8)	0.0133(5)	0.0125(4)	0.0123(5)	0.0150(6)	0	0	0
Al2	4c	1/2	0.1512(4)	1/4	1.0	0.013(2)	0.013(17)	0.015(2)	0.011(2)	0	0	0
Al3	8e	0.2309(4)	1/2	0	0.96(1)	0.014(1)	0.014(10)	0.013(1)	0.015(2)	0	0	0.00(1)
$CeAuAl_3$, space group *I4mm*, a = 4.3364(4) Å, c = 10.850(2) Å												
Ce1	2a	0	0	0	1.0	0.0078(7)	0.0068(6)	0.0068(6)	0.0099(7)	0	0	0
Au1	2a	0	0	0.6356(2)	1.0	0.0124(6)	0.0137(6)	0.0137(6)	0.0099(5)	0	0	0
Al1	2a	0	0	0.406(1)	1.0	0.008(3)	0.003(2)	0.003(2)	0.017(4)	0	0	0
Al2	4b	0	1/2	0.2608(7)	1.0	0.009(3)	0.005(3)	0.011(3)	0.012(3)	0	0	0
$CeCuAl_3$, space group *I4mm*, a = 4.2508(4) Å, c = 10.644(1) Å												
Ce1	2a	0	0	0	1.0	0.0063(4)	0.0058(4)	0.0058(4)	0.0071(5)	0.000	0.000	0.000
Cu1	2a	0	0	0.6314(3)	0.84(4)	0.008(1)	0.009(1)	0.009(1)	0.008(2)	0.000	0.000	0.000
Al1	2a	0	0	0.6314(3)	0.16(4)	0.008(1)	0.009(1)	0.009(1)	0.008(2)	0.000	0.000	0.000
Al2	2a	0	0	0.4040(8)	1.0	0.009(1)	0.006(2)	0.006(2)	0.015(3)	0.000	0.000	0.000
Al3	4b	0	1/2	0.2489(6)	0.94(4)	0.008(1)	0.008(3)	0.009(3)	0.008(1)	0.000	0.000	0.000
$CePtAl_3$, space group *I4mm*, a = 4.3239(4) Å, c = 10.667(2) Å												
Ce1	2a	0	0	0	1.0	0.009(1)	0.008(1)	0.008(1)	0.009(2)	0.00000	0.00000	0.00000
Pt1	2a	0	0	0.6364(3)	0.82(1)	0.011(1)	0.013(1)	0.013(1)	0.007(1)	0.00000	0.00000	0.00000
Al1	2a	0	0	0.6364(3)	0.18(1)	0.011(1)	0.013(1)	0.013(1)	0.007(1)	0.00000	0.00000	0.00000
Pt2	2a	0	0	0.386(1)	0.82(1)	0.034(5)	0.021(3)	0.021(3)	0.060(8)	0.00000	0.00000	0.00000
Al2	2a	0	0	0.386(1)	0.18(1)	0.034(5)	0.021(3)	0.021(3)	0.060(8)	0.00000	0.00000	0.00000
Al3	4b	0	1/2	0.257(1)	1.0	0.011(5)	0.010(5)	0.013(5)	0.011(4)	0.00000	0.00000	0.00000

Table 4: Refined fractional atomic coordinates, site occupations as well as equivalent and anisotropic thermal displacement parameters for $CeAgAl_3$, $CeAuAl_3$, $CeCuAl_3$ and $CePtAl_3$.

Atom	Wyckoff	x/a	y/b	z/c	sof	u_{eq}
(3a) $CePdAl_3$, space group *I4mm*, a = 12.988(1) Å, c = 10.589(1) Å						
Ce1	2a	0	0	0	1.0	0.013(2)
Ce2	8d	0.3333(4)	0	0.0189(9)	1.0	0.009(1)
Ce3	8c	0.3291(4)	0.32918	0.012(2)	1.0	0.013(1)
Pd1	2a	0	0	0.649(2)	1.0	0.009(1)
Pd2	8d	0.5	0.1653(5)	0.875(2)	1.0	0.014(3)
Pd3	8c	0.1696(5)	0.16963	0.155(2)	0.65(2)	0.010(3)
Al1	8c	0.1696(5)	0.16963	0.155(2)	0.34(2)	0.010(3)
Al2	2a	0	0	0.422(3)	0.78(7)	0.010(3)
Pd4	2a	0	0	0.422(3)	0.21(7)	0.010(3)
Al3	4b	0.5	0	0.262(6)	1.0	0.008(9)
Al4	8d	0.5	0.1687(9)	0.102(2)	0.80(3)	0.019(6)
Pd5	8d	0.5	0.1687(9)	0.102(2)	0.19(3)	0.019(6)
Al5	8d	0.5	0.339(3)	0.257(5)	1.0	0.009(8)
Al6	8d	0.159(3)	0	0.271(5)	1.0	0.015(9)
Al7	8c	0.154(2)	0.15476	0.882(4)	1.0	0.024(6)
Al8	16e	0.347(2)	0.168(2)	0.260(3)	1.0	0.008(5)
($BaNiSn_3$) $CePdAl_3$*, space group *I4mm*, a = 4.34396(6) Å, c = 10.5915(2) Å						
Ce1	2a	0	0	0	1.0	0.0316(8)
Pd1	2a	0	0	0.6247(4)	1.0	0.0410(1)
Al1	2a	0	0	0.349(1)	1.0	0.011(1)
Al2	4b	0	1/2	0.2579(8)	1.0	0.011(1)

Table 5: Refined fractional atomic coordinates, site occupations as well as isotropic thermal displacement parameters for two modifications of $CePdAl_3$. *results were obtained by the evaluation of X-ray powder diffraction data

Highlights for "Single crystal growth of Ce*T*Al_3 (*T* = Cu, Ag, Au, Pd and Pt)

- Single crystal growth in float zone technique of Ce*T*Al_3 (*T* = Cu, Ag, Au, Pd and Pt).
- Crystal structure is *I4mm* for *T* = Au, Cu, Pt, Pd.
- $CePdAl_3$ shows a three-fold multiplied parameter *a*.
- Orthorhomic distortion to *Cmcm* structure is found for *T*=Ag.
- No magnetic order is found for *T* = Pt, Pd down to 100mK.